Pergamon

Appl. Math. Lett. Vol. 10, No. 2, pp. 39–44, 1997

0893-9659/97 $17.00 + 0.00

PII: S0893-9659(97)00008-6

Renal Concentrating Mechanism: Central Core and Vasa Recta Models

R. P. TEWARSON AND I. H. MOON
Institute of Mathematical Modeling
Department of Applied Mathematics and Statistics
State University of New York
Stony Brook, NY 11794-3600, U.S.A.

(Received June 1996; accepted August 1996)

Abstract—Mathematical models are essential in testing alternative hypotheses to explain the concentrating mechanism of the mammalian kidney. The basis features of a central core and two other vasa recta models, as well as efficient modeling techniques are described. It is shown that, by suitable choice of a few parameters, the two vasa recta models lead to the same osmolality and concentration ratios as the central core model.

Keywords—Kidney models, Differential equations, Numerical methods.

INTRODUCTION

In mammals, the kidney is used to maintain the volume and composition of body fluids within very narrow limits. Mathematical models have been responsible for many of the basic ideas leading to our understanding of this mechanism. A lengthwise cross-section of the kidney reveals two distinct parts: the *cortex* and the *medulla*. The medulla is subdivided into the *outer* and the *inner* parts. The cortex contains the renal corpuscles, and the proximal and the distal tubules. The loops of Henle (which turn at different levels) and the collecting ducts reside in the medulla. Blood gets filtered in the renal corpuscle; the filtrate then flows successively through the proximal tubule (which winds around the renal corpuscle), Henle's loop (the descending and ascending parts are joined by a hairpin turn), the distal tubule (which winds around in the cortex and makes contact with the *Juxta-glomerular apparatus* related to the renal corpuscle), and the collecting duct to emerge as the final urine. Blood also flows down into the medulla and then back to the cortex through the *vasa recta*. This retrieves the water and solutes absorbed from the tubules. By varying the composition of the final urine, the composition of the interstitial fluid bathing the cells of the body is maintained within the narrow limits compatible with life.

Computer models that use experimentally available parameters have generated concentration gradients in the outer medulla consistent with experimental data by including metabolically driven (active) salt transport out of thick ascending limb of Henle's loop, but have been unable to generate any significant concentration gradient in the inner medulla where there is no active transport. How the inner medulla concentrates urine is still one of the major unsolved problems in renal physiology. Hypotheses continue to be proposed to answer this question. Mathematical

Research supported by NIH Grant DK17593.

models are essential in the testing of such alternate hypotheses. See [1] for more details and an extensive list of references.

The loops of Henle (each loop consists of a descending and an ascending part—DHL and AHL) turn at various medullary levels. In some models [2,3], this fact is incorporated by merging all the loops into a single composite loop, and allowing part of the axial flow at each level to be shunted from DHL to AHL. Such models are called Shunt Models—SM. Naturally, in such models, the cross-sectional areas of the DHL and AHL, in the composite loop, progressively decrease in accordance with the original nephron distribution. The vasa recta have a shunting mechanism via the capillaries. This fact has been utilized to develop a composite vas rectum with shunts [4,5]. Some models have utilized multi-vasa recta [2,3].

Multinephron models, all of which use Stephenson's central core assumption [6], have also been developed. Two representations have been used in such models. One is to use a small number (no more than six) of discrete loops of Henle [7–10]. The other is to use a continuous distribution of loops represented by weighting the integrals when computing convective and transmural fluxes [7,11,12].

It has been observed that a central core model concentrates better than the corresponding vasa recta model. In particular, for a model of the inner medulla, where the Central Core (CORE) is replaced by one Descending Vas Rectum (DVR), two Ascending Vasa Recta (AVR) and two nodes, it was shown in [13] that concentrating ability decreases with increasing vasa recta flow.

In this paper, we present detailed comparative studies between our central core model ($4t$) and two other vasa recta models ($6t$) and ($7t$). Model $4t$, which is shown in Figure 1 and described in detail in [14], has four tubes: DHL, AHL, collecting duct (CD), and CORE. As already mentioned, the loop distribution is approximated by shunts (shown by dotted lines in Figure 1) from DHL to AHL. It was shown in [15] that this is a reasonable approximation. Model $6t$ (see Figure 2) is obtained from model $4t$ by replacing the CORE by one DVR and two AVRs. Model $7t$, shown in Figure 3, results from $6t$ by replacing the two AVRs by three AVRs. Both models, $6t$ and $7t$, differ from models in [3,13,16–18], in that the so-called *nodes* are not included, since it was shown in [13,16,17] that the effect of nodes is mitigated when realistic diffusion is included. In the $7t$ model, we have made use of Figure 1d in [19, p. 540], where the AVRs can be classified into three categories:

(a) those near AHL and CD,
(b) those near DHL and AHL, and
(c) those belonging to neither categories (a) or (b).

MODEL $4t$

For this model (see Figure 1 and for more details see [19]), let $i = 1, 2, 3$, and 4 denote, respectively, DHL, AHL, CD, and CORE, and x be the distance measured from the top ($x = 0$) to the bottom ($x = 1$). The variables are: $F_{iv}(x)$ = volume flows, $C_{ik}(x)$ = solute concentrations, where $k = s$ (salt), u (urea). The entering flows and concentrations $F_{1v}(0)$, $C_{1k}(0)$, $F_{3v}(0)$, and $C_{3k}(0)$ are given. Also, $F_{4v}(1) = 0$, $C'_{4k}(1) = 0$; at $x = 1$, DHL (tube 1) makes a hairpin turn to become AHL (tube 2), and therefore, $F_{2v}(1) = -F_{1v}(1)$ and $C_{2k}(1) = C_{1k}(1)$.

The differential equations are

$$\frac{dF_{iv}}{dx} + J_{iv}(x) = 0, \tag{1}$$

$$\frac{d(F_{iv}C_{ik})}{dx} + J_{ik}(x) = 0, \qquad i \neq 4 \tag{2}$$

$$\frac{dF_{4k}}{dx} + J_{4k}(x) = 0, \tag{3}$$

$$D_{4k}\frac{dC_{4k}}{dx} + F_{4k} - F_{4v}C_{4k} = 0, \tag{4}$$

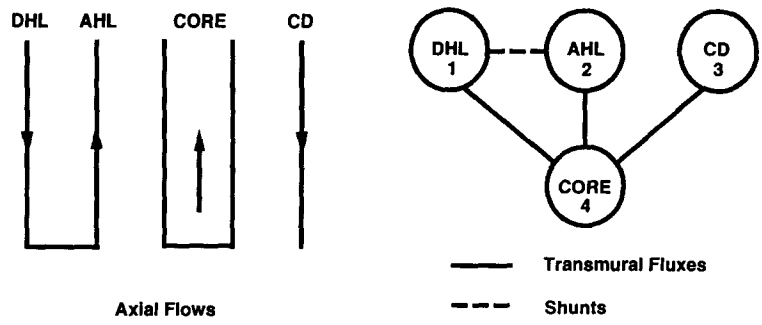

Figure 1. Four tube central core model ($4t$).

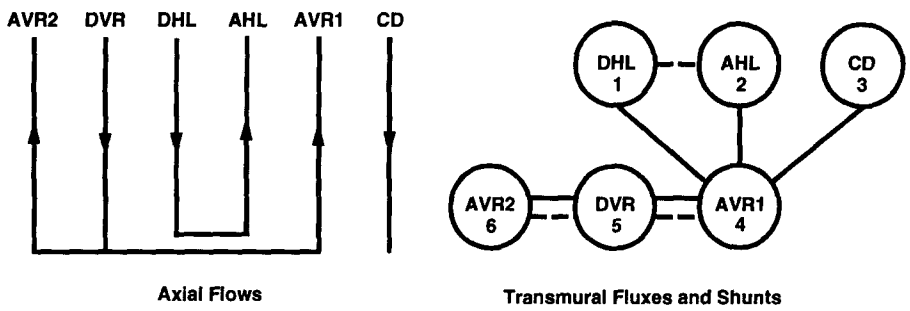

Figure 2. Six tube vasa recta model ($6t$).

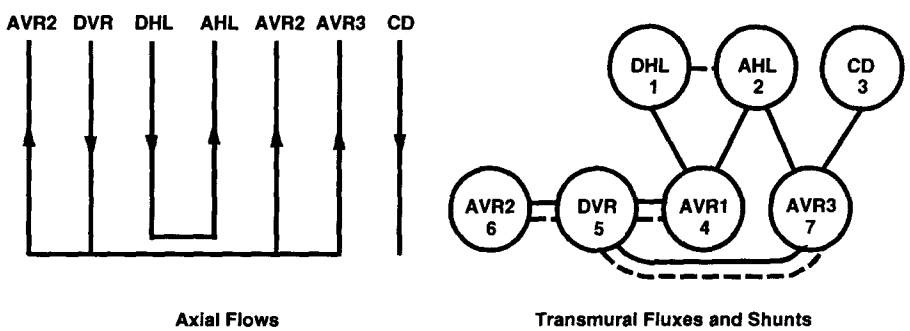

Figure 3. Seven tube vasa recta model ($7t$).

where $J_{iv}(x)$ and $J_{ik}(x)$ are, respectively, transmural volume and solute fluxes, D_{4k} are the diffusion coefficients, and $F_{4k}(x)$ are the axial solute flows, $J_{iv}(x)$ and $J_{ik}(x)$ are functions of only $C_{ik}(x)$ and $C_{4k}(x)$, and are given by

$$J_{iv}(x) = h_{iv}(x) \sum_{k} RT \left[C_{4k}(x) - C_{ik}(x)\right] \sigma_{ik}(x), \qquad k = 1, 2, \tag{5}$$

$$J_{ik}(x) = J_{iv}(x) \left[1 - \sigma_{ik}(x)\right] \frac{C_{ik}(x) + C_{4k}(x)}{2} + h_{ik}(x) \left[C_{ik}(x) - C_{4k}(x)\right] + \frac{a_{ik}(x)}{1 + \left(b_{ik}(x)/C_{ik}(x)\right)}, \qquad k = 1, 2, \tag{6}$$

where σ_{ik} is the Staverman reflection coefficient of the wall of the i^{th} tube for the k^{th} solute, h_{ik} is its passive permeability for the k^{th} solute, h_{iv} is its hydraulic permeability coefficient, a_{ik} is the maximum rate of transport, b_{ik} is Michaelis constant, R is the gas constant, and T is the absolute temperature.

Mass balance requires that

$$\sum_{i=1}^{4} J_{iv}(x) = 0, \qquad \sum_{i=1}^{4} J_{ik}(x) = 0. \tag{7}$$

If we set $h = 1/n$, $x_j = (j-1)h$, where $j = 1, \ldots, n+1$; $F_{ivj} = F_{iv}(x_j)$, $F_{ikj} = F_{ik}(x_j)$, and $C_{ikj} = C_{ik}(x_j)$, then, as shown in [14], integrating (1)–(4) and using the boundary conditions, we get

$$f(y, z) = 0, \tag{8}$$

$$g(y, z) = 0, \tag{9}$$

where $y = (C_{ikj})$, $i = 1, 2, 3$, $k = s, u$; for $i = 1, 3$, $j = 2, \ldots, n+1$; and for $i = 2$, $j = n, n-1, \ldots, 1$; $z = (C_{4kj})$, $k = s, u$; $j = 1, \ldots, n+1$. Evidently, $f, y \in R^{6n}$ and $z, g \in R^{2(n+1)}$.

It is shown in [14] that the sparsity of equations (8) makes it possible to express y, called the nonbasic variable, as a function of the basic variable z by solving the $f(y(z), z) = 0$ for $y(z)$. This leads to efficient solution of the basic equation $g(y(z), z) = 0$ for z. Detailed mathematical analysis of such nonlinear Shur complement methods is given in [20].

MODEL 6t

The differential equation for this model is equation (1),

$$\frac{d(F_{iv}C_{ik})}{dx} + J_{ik}(x) = 0, \tag{10}$$

and equation (3). The boundary values $F_{iv}(0)$, $C_{ik}(0)$, $i = 1, 3, 5$, $k = s, u$ are given. The rest of the boundary values are obtained from the conditions: $F_{2v}(1) = -F_{1v}(1)$, $C_{2k}(1) = C_{1k}(1)$, $C_{4k}(1) = C_{5k}(1) = C_{6k}(1)$, $F_{4v}(1) = -\gamma_4 F_{5v}(1)$, $F_{6v}(1) = -(1-\gamma_4)F_{5v}(1)$, where γ_4 is the fraction of DVR (tube 5) volume flow to AVR1 (tube 4). For $i = 1, 2, 3$, and 5, J_{iv} and J_{ik} are given by equations (5) and (6). The transmural fluxes between DVR and AVR2 are given by analogous equations with $C_{4k}(x)$ replaced by $C_{6k}(x)$. In the mass balance equations (7), the upper limit for the i sum is, obviously, now 6.

In our computational algorithms, we choose the equations and variables for AVR1 and DVR as basic. Thus, we let $y = (C_{ikj})$, $i = 1, 2, 3, 6$, $k = s, u$; for $i = 1, 3$, $j = 2, \ldots, n+1$ and for $i = 2, 6$, $j = n, n-1, \ldots, 1$; $z = (F_{5vj}, C_{ikj})$, $k = s, u$; for $i = 4$, $j = 1, \ldots, n$, and for $i = 5$, $j = 2, \ldots, n+1$. Therefore, in equations (8) and (9), $f, y \in R^{8n}$ and $z, g \in R^{5n}$.

MODEL 7t

This model (see Figure 3) is obtained from model 6t by replacing AVR1 (tube 4) with two AVRs—AVR1 (tube 4) and AVR3 (tube 7). This requires additional equations for transmural fluxes between DVR and AVR3, and change in i sum limit in equation (7) from 4 to 7. The other changes are in the boundary conditions: $C_{4k}(1) = C_{5k}(1) = C_{6k}(1) = C_{7k}(1)$, $F_{7v}(1) = -\gamma_7 F_{5v}(1)$, $F_{6v}(1) = -(1-\gamma_4-\gamma_7)F_{5v}(1)$. The basic equations and variables are the ones associated with DVR, AVR1, and AVR3. Thus, we let $y = (C_{ikj})$, $i = 1, 2, 3, 6$, $k = s, u$; for $i = 1, 3$, $j = 2, \ldots, n+1$, and for $i = 2, 6$, $j = n, n-1, \ldots, 1$; $z = (F_{5vj}, C_{ikj})$, $k = s, u$; for $i = 4, 7$, $j = 1, \ldots, n$, and for $i = 5$, $j = 2, \ldots, n+1$. Therefore, in equations (8) and (9), $f, y \in R^{8n}$ and $z, g \in R^{7n}$.

COMPUTATIONAL RESULTS

We used the same boundary conditions and parameters as in [3,13,16–18]. The results are given in Table 1, where $F_{5v}(0)$ is the DVR input volume flow, γ_4 and γ_7 are, respectively, the fractions

of the DVR volume flows going up AVR1 and AVR3 at $x = 1$; α_{i5}, $i = 1, 2$, and 3, represent the fractions of total possible transmural fluxes, J_{i5}, between DHL and DVR, AHL and DVR, and CD and DVR. The osmolatity, salt and urea concentrations ratios between bottom ($x = 1$) and top ($x = 0$) are given in the last six columns. The boldface lines are the initial results with the original $F_{5v}(0)$, with the DVR volume flow equally distributed among the AVRs. Thus, $6t$ and $7t$ have smaller values than $4t$, for all these ratios. After extensive computational experiments, we found that by modifying only $F_{5v}(0)$, γ_4, and γ_7, we were able to get the ratios, given in the third and sixth lines. Obviously, these are not close enough to those for $4t$. However, by choosing small values for α_{i5}, we got the corresponding ratios (lines four and seven) reasonably close to those obtained by model $4t$ in line one.

Table 1. Osmolality and concentration ratios between values at $x = 1$ and $x = 0$.

							DHL (Tube 1)			CD (Tube 3)		
	$F_{5v}(0)$	γ_4	γ_7	α_{15}	α_{25}	α_{35}	Osm.	Salt	Urea	Osm.	Salt	Urea
$4t$	–	–	–	–	–	–	**2.641**	**1.944**	**14.206**	**1.703**	**6.429**	**0.716**
	3.440D-7	0.50	–	–	–	–	**2.340**	**1.776**	**11.701**	**1.507**	**5.891**	**0.591**
$6t$	1.656D-7	0.50	–	–	–	–	2.648	1.968	13.940	1.687	6.462	0.688
	1.570D-7	0.50	–	0.0711	0.0711	0.0822	2.680	2.000	13.989	1.703	6.424	0.716
	3.440D-7	0.25	0.25	–	–	–	**2.391**	**1.805**	**12.120**	**1.537**	**5.937**	**0.617**
$7t$	2.100D-7	0.45	0.20	–	–	–	2.606	1.934	13.763	1.665	6.306	0.695
	2.200D-7	0.45	0.20	0.0156	0.0156	0.0560	2.666	1.978	14.090	1.703	6.425	0.716

REFERENCES

1. J.L. Stephenson, Urinary concentration and dilution: Models, In *Handbook of Physiology*, (Edited by E. Windhager), Chapter 30, pp. 1349–1408, Oxford University Press, New York, (1992).
2. L.C. Moore and D.L. Marsh, How descending limb of Henle's loop permeability effects hypertonic urine formation, *Am. J. Physiol.* **239**, F57–71, (1980).
3. A.S. Wexler, R.E. Kalaba and D.H. Marsh, Three-dimensional anatomy and renal concentrating mechanism—I. Modeling results, *Am. J. Physiol. (Renal Fluid Electrolyte Physiol. 29)* **260**, F368–F383, (1991).
4. P.S. Chandhoke and G.M. Saidel, Mathematical model of mass transport throughout the kidney: Effects of nephron heterogeneity and tubular-vascular organization, *Ann. Biomed. Engr.* **9**, 263–501, (1983).
5. J.A. Jacquez, D. Foster and E. Daniels, Solute concentration in the kidney—I. A model of the renal medulla and its limit cases, *Math. Biosci.* **32**, 307–335, (1976).
6. J.L. Stephenson, Concentration of urine in a central core model of the renal counterflow system, *Kidney Int.* **2**, 85–94, (1972).
7. H.E. Layton, Urea transport in a distributed loop model of the urine concentrating mechanism, *Am. J. Physiol. (Renal Fluid Electrolyte Physiol. 27)* **258**, F1110–F1124, (1990).
8. R. Mejia and J.L. Stephenson, Numerical solution of multinephron kidney equations, *J. Computational Physics.* **32**, 235–246, (1979).
9. R. Mejia and J.L. Stephenson, Solution of a multinephron, multisolute model of the mammalian kidney by newton and continuation methods, *Math. Biosci.* **68**, 279–298, (1984).
10. J.L. Stephenson, Y. Zhang and R.P. Tewarson, Electrolyte, urea, and water transport in a two nephron central core model of the medulla, *Amer. J. of Physiology* **25**, F399–F413, (1989).
11. H.E. Layton, Distribution of Henle's loops may enhance urine concentrating capability, *Biophys. J.* **49**, 1033–1040, (1986).
12. H.E. Layton, Concentrating urine in the inner medulla of the kidney, *Comments Theoretical Biology* **1**, 179–196, (1989).
13. J.L. Stephenson, H. Wang and R.P. Tewarson, Effect of vasa recta flow on concentrating ability of the renal inner medulla, *Amer. J. of Physiology* **268** (4), F698–F709, (1995).
14. R.P. Tewarson, H. Wang, J.L. Stephenson and J.F. Jen, Efficient solution of differential equations for kidney concentrating mechanism analyses, *Appl. Math. Lett.* **4** (6), 69–72, (1991).
15. H. Wang, J.L. Stephenson, Y. Deng and R.P. Tewarson, An efficient parallel algorithm for solving n-nephron models of the renal inner medulla, *Computers Math. Applic.* **28** (5), 1–12, (1994).
16. J.F. Jen, H. Wang, R.P. Tewarson and J.L. Stephenson, Comparison central core and radially separated models of the renal inner medulla, *Amer. J. of Physiology* **268** (4), F693–F697, (1995).
17. J.L. Stephenson, J.F. Jen, H. Wang and R.P. Tewarson, Convective uphill transport of nacl from ascending thin limb of the loop of Henle, *Amer. J. of Physiology* **268** (4), F680–F692, (1995).

18. A.S. Wexler, R.E. Kalaba and D.H. Marsh, Three-dimensional anatomy and renal concentrating mechanism—II. Sensitivity results, *Am. J. Physiol. (Renal Fluid Electrolyte Physiol. 29)* **260**, F384–F394, (1991).
19. K.V. Lemley and W. Kriz, Cycles and separations: The histotopography of the urinary concentrating process, *Kidney Internat.* **31**, 538–548, (1987).
20. R.P. Tewarson, J.L. Stephenson and L.L. Juang, A note on solution of large sparse systems of nonlinear equations, *J. Math. Anal. and Appl.* **63**, 439–445, (1978).